geoconvention
Calgary • Canada • May 11-13 2026

Beyond the 002 peak: Advanced XRD strategies for industrial graphite characterization and graphitization assessment

Reza, Deevsalar
Department of Mineralogy, AGAT Laboratories Ltd., 1620 27 Ave NE Calgary, AB T2E 8W4

Graphite's layered sp²-bonded structure is the foundation of its widespread application as an anode material in lithium-ion batteries and other advanced energy storage devices. The electrochemical performance of graphite is controlled by its microstructural signatures, such as stacking order, crystallite coherence, defect density, and degree of graphitization (DoG). The analysis of analysis of basal (002) reflection in X-ray diffraction (XRD) data is the most widely applied method for graphite characterization. However, the pronounced structural and morphological heterogeneity in graphite powders, including preferred orientation effects and particle-size–dependent peak asymmetry complicates interpretation of bulk XRD data. This study introduces an integrated XRD-based framework that extends beyond conventional single-peak analysis of the (002) reflection and resolves graphite stacking heterogeneity. Two bulk graphite samples and associated particle-size–fractionated subsamples, representative of partially processed synthetic graphite samples, were analyzed using full-pattern Rietveld refinement incorporating preferred orientation correction, anisotropic size–strain models, and constrained multi-domain graphite structures. Diffraction-based averaging strategies were applied to derive phase-weighted and mass-weighted interlayer spacing required for DoG calculation. Results show that raw graphite powders contain coexisting graphite populations with distinct stacking order and degrees of graphitization that correlates with particle size distribution (PSD). It confirms that particle size fractionation acts as a structural sorting process, with fine fractions (<75 µm) enriched in less-ordered graphite domains and amorphous carbon, while intermediate fractions (75–150 µm) retain a higher proportion of well-ordered graphite in pre-treatment graphite powders. The results further clarify that size-resolved DoG analyses provide complementary diagnostic insight when greater microstructural resolution is required, whereas bulk DoG values remain structurally meaningful, diffraction-weighted averages. The Mass-weighted reconstruction translate the heterogeneity resolved by size-resolved DoG analysis into a representative bulk DoG value. This approach also provides insight into the ability of particle size reduction techniques to preserve basal-plane stacking in thermally treated graphite. The proposed framework is a transparent and defensible approach allowing comprehensive graphite characterization and is readily transferable to routine laboratory and industrial workflows.

1. Introduction

Graphite's unique layered structure, composed of sp^2-bonded graphene sheets stacked along the c-axis, provides exceptional electrical conductivity, thermal stability, and chemical robustness (Franklin, 1951; Chung, 2002). These properties enable its widespread use as the dominant anode material in lithium-ion batteries and in a range of other industrial applications. Graphite microstructural parameters, particularly stacking order, crystallite dimensions, defect density, and degree of graphitization (DoG) closely linked to its electrochemical performance metrics, such as rate capability, irreversible capacity loss, and long-term cycling stability (Inagaki & Kang, 2014).

X-ray diffraction (XRD) is the most widely applied technique for assessing graphite structure, with the basal (002) reflection commonly used to estimate interlayer spacing and calculate the DoG. In practice, however, graphite powders rarely represent structurally uniform materials. Natural, synthetic, and processed graphites frequently contain coexisting stacking populations with slightly different interlayer spacings, partially turbostratic domains, amorphous carbon, and minor crystalline impurities (Warren, 1941; Franklin, 1951; Biscoe & Warren, 1942). In addition, the graphite's platy particle morphology and broad particle size distributions promotes preferred orientation, particle-size–dependent absorption (heterogeneity), and asymmetric diffraction peak profiles (Klug & Alexander, 1974).

As a result, diffraction patterns collected for different aliquots of the identical bulk graphite samples may vary depending on subsampling, packing behavior, and particle size distribution. While bulk XRD analysis remains valid and widely useful for routine quality control and benchmarking practices, the resulting DoG values must be interpreted with an understanding of the structural averaging occurring across the diffraction measurement. In particular, the occurrence of asymmetric (002) peak profiles and particle size-dependent peak shifts suggest that bulk graphite often consists of distinct stacking populations rather than a single homogeneous structural state (Warren, 1941; Scarlett & Madsen, 2006).

This study introduces and applies an integrated XRD-based methodology that goes beyond traditional (002) peak analysis allowing the resolution of graphite stacking heterogeneity, without sacrificing the validity of routine bulk measurements. A combination of optimized sample preparation, full-pattern Rietveld refinement, constrained multi-domain graphite models, and diffraction-based averaging strategies has been used to clarify the structural meaning of bulk DoG values and to provide additional diagnostic insight through particle-size–resolved analysis.

2. Materials and Methods

2.1. Graphite samples and particle size fractionation

In order to evaluate the influence of particle size distribution on XRD response and key microstructural parameters, two representative samples of partially processed synthetic graphite, typical of materials produced in industrial applications, were selected for this study. Each bulk sample was dry-sieved into three discrete particle size fractions (<75 µm, 75–150 µm, and 150–425 µm), and mass fraction of each size class was recorded for subsequent mass-weighted averaging. The bulk graphite samples were analyzed along with subsamples to compare routine

bulk measurements with reconstructed bulk properties derived from size-resolved analysis and investigate the subsampling effect.

2.2. Sample preparation for X-ray diffraction

A critical step in the workflow was the preparation of powder specimens using consistent loading procedures to ensure comparability between bulk and size-fractionated samples. Given the tendency of platy materials to develop preferred orientation, graphite powders were lightly packed into sample holders to avoid excessive compaction (e.g., Klug & Alexander, 1974). The sample preparation procedure comprised the following steps:

- Samples were oven-dried at 60 °C to remove free moisture.
- Each sample was thoroughly homogenized, and a representative subsample (~3 g) was gently de-agglomerated using a hand-held agate mortar and pestle.
- The powder was then carefully loaded into an XRD sample holder to minimize preferred orientation.
- To quantify the amorphous content and ensure accurate determination of graphitization parameters, Rietveld refinement (Rietveld, 1969; Bish & Post 1993) was performed on mixtures of graphite with an internal standard (zincite, ZnO).

2.3. X-ray diffraction data collection

XRD measurements were carried out using a Bruker D8 Endeavor diffractometer equipped with a cobalt radiation source (Co Kα). Data were collected over an angular range sufficient to capture basal and non-basal graphite reflections as well as potential impurity phases. Scan parameters (Table 1) were held constant across all measurements to ensure comparability, following standard laboratory practice for polycrystalline materials in Mineralogy Department of the AGAT Laboratories Ltd.

Table 1. The Instrumentation and operating conditions.

Parameter	Specification
Diffractometer	Bruker D8 Endeavor
Radiation source	Co Kα (λ = 1.78897 Å)
Scan range (2θ)	5°–80°
Step size	0.02°
Counting time	1.0 s per step
Detector	LynxEye XCT
Operating voltage/current	35 kV / 40 mA

2.4. Data Processing

XRD data were processed using Bruker TOPAS for Rietveld refinement and PANalytical HighScore for phase identification. Phase identification was carried out by peak matching, profile fitting, and refinement of structural models using reference patterns from the ICDD PDF-5 Minerals database (2026). Quantitative phase analysis was performed by Rietveld refinement employing crystallographic information files (STR) obtained from the ICDD database. Refinement parameters included scale factors, background functions, unit-cell dimensions, peak-shape

parameters, preferred orientation, instrumental broadening, and, where necessary, atomic positions.

2.4.1. Rietveld refinement strategy

As previously noted, full-pattern Rietveld refinements were carried out using Bruker AXS TOPAS-64 V7.13 (version 7.0.0.7) software following established methodology (Young, 1993). Graphite was modeled using its standard crystal structure, and preferred orientation effects were addressed using a March–Dollase function applied along the [001] direction (Dollase, 1986). Where necessary, anisotropic size–strain models were applied to account for stacking disorder and direction-dependent broadening.

The bulk graphite samples usually display asymmetric (002) peak profiles which complicates accurate fitting. To overcome the fitting challenges posed by the asymmetric (002) peak profiles, a constrained multi-domain graphite model was employed. In this approach, two graphite domains sharing identical basal lattice parameters and atomic positions were refined simultaneously, with independent refinement of the lattice parameter c to represent distinct stacking populations with slightly different interlayer spacings. The constrained multi-phase approach is a well-established technique for resolving overlapping diffraction features and mixed structural populations (Scarlett & Madsen, 2006).

2.4.2. Diffraction-based metrics and degree of graphitization

The interlayer spacing d_{002} was calculated from the refined lattice parameter ″c″ for each graphite domain identified in the sample. The DoG was calculated from d_{002} using a literature-defined reference scale bounded by ideal graphite (i.e., perfectly crystalline graphite, typically defined by the well-accepted interlayer spacing $d_{002} \approx 3.354A^{\circ}$) and poorly ordered turbostratic carbon (i.e., corresponds to highly disordered carbon $d_{002} \approx 3.44–3.50A^{\circ}$), consistent with classical graphitization models (Franklin, 1951).

For size-fractionated samples, phase-weighted averaging ($d_{002,fraction} = \sum(w_i \cdot d_{002,i})$, where w_i= weight fraction of phase i), within individual diffraction patterns and mass-weighted averaging ($d_{002,bulk} = \sum(m_{j \cdot d002,j})$, where m_j = mass fraction of size class j), across particle size fractions were applied to reconstruct representative bulk interlayer spacing and DoG values. This approach reflects the contribution of each size fraction to the bulk properties of the graphite samples, overcoming the misrepresentation caused by a simple arithmetic average.

3. Results and Discussion

3.1. Diffraction behavior across particle size fractions

As shown in Fig.1, a systematic variations in the basal (002) reflection are observed as a function of particle size fraction on diffractogram for three fractions classes (<75 µm, 75–150 µm, and 150–425 µm) studied in this research. Differences in peak position, intensity, and asymmetry persist despite identical preparation and acquisition conditions, indicating an intrinsic microstructural heterogeneity rather than experimental artifacts (e.g., Warren, 1941; Franklin, 1951).

While observed intensity variations across size fractions are consistent with graphite's platy morphology and its tendency toward preferred orientation during powder mounting (e.g., Klug & Alexander, 1974), it does not directly alter d-spacing value. Particle alignment was corrected using March-Dollase model (Dollase, 1986), so that variations in peak intensity were not misinterpreted as changes in graphite structure. On the other hand, systematic shifts in the (002) peak position in the analyzed sub-samples (Fig. 1) indicates that particle size fractionation segregates graphite domains with different stacking order. Fine fractions (<75 μm) exhibit larger interlayer spacings characteristic of less ordered or defect-rich stacking, while intermediate fractions (75–150 μm) retain smaller d_{002} values indicative of more ordered graphite (e.g., Franklin, 1951; Inagaki & Kang, 2014).

Likewise, the asymmetric (002) peak profiles can be explained by the coexistence of multiple graphite stacking populations rather than isotropic size broadening or instrumental effects (e.g., Warren, 1941). Constrained multi-domain Rietveld refinement resolves these profiles into physically meaningful stacking populations, consistent with established approaches for mixed or overlapping diffraction features (e.g., Scarlett & Madsen, 2006).

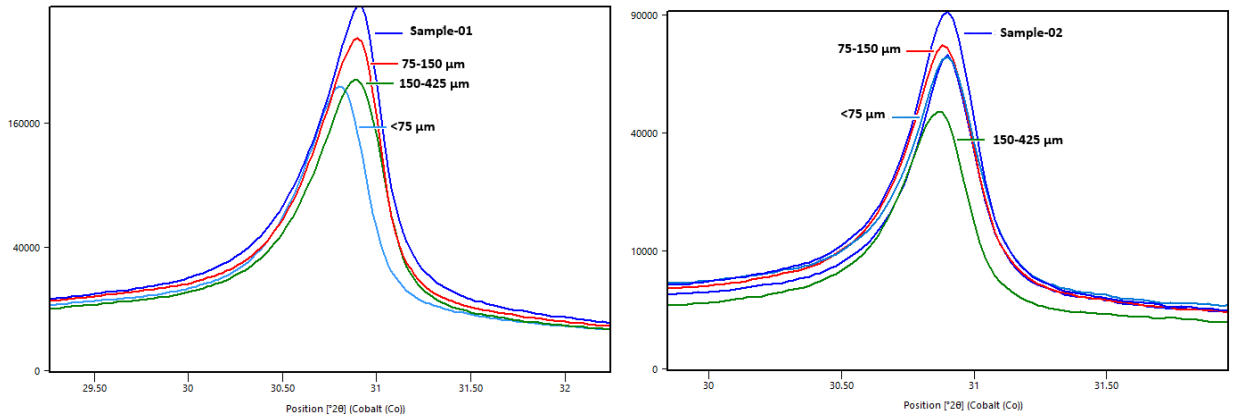


Fig.1. Comparison of the basal (002) XRD peak profiles for two graphite samples measured using Co Kα radiation. For each sample, the diffraction profile of the bulk material is shown together with those of particle size–fractionated subsamples (e.g., <75 μm, 75–150 μm, and 150–425 μm). Systematic differences in peak position, intensity, and asymmetry among size fractions highlight size-dependent variations in interlayer spacing and structural order within each graphite sample.

3.2. Degree of Graphitization and diffraction-based averaging

Size-resolved analysis results for the selected population of the samples (Table 2) reveals that among two graphite domains, Graphite-I consistently exhibit higher DoG values (diffraction weighted average), while Graphite-II, associated with the left-shoulder features of the (002) reflection, display lower DoG values and are enriched in fine fractions alongside amorphous carbon. In the bulk sample-01, 2.0 g out of 3.0 g lies in the < 75 μm fraction that has the average fraction-specific DoG (~ 89.2%), but comprises ~ 67% of the bulk mass, thereby pulls the reconstructed mass-weighted bulk DoG down to 88.6% (Δ_{DoG} = -4.5, Table 2). In comparison,

bulk phase-weighted DoG for sample-02 (90.1) increases to a reconstructed mass-weighted bulk DoG of 94.6, since the intermediate fraction class (i.e., 150-425 μm) forms ~ 61% of the bulk mass and poses the highest fraction-specific DoG (~ 95.1), that exerted strong upward impact on the mass-weighted bulk DoG (Δ_{DoG} = +4.5, Table 2). This confirms that bulk DoG values alone cannot reliably estimate representative graphitization without consideration of how structurally distinct graphite populations are distributed across the particle size fractions present in the bulk sample.

Bulk DoG values remain internally consistent and reproducible for the aliquots from the same bulk powder when consistent preparation and measurement protocols are applied; however, size-resolved analysis clarifies that these bulk values arise from mixtures of structurally distinct graphite populations and disordered components (e.g., Franklin, 1951). The observed differences in DoG values and amorphous content distributions between different samples (Table 2) are not random, as they reflect the distinct microstructural "fingerprints" reflecting differences in synthesis history, thermal treatment, or mechanical processing of the graphite samples (Inagaki & Kang, 2014), which are of direct relevance to industrial applications.

Accordingly, the contrast between Sample-01 (fine-dominated) and Sample-02 (coarse-dominated) reflects differences in processing history and structural heterogeneity.

Worth to note that under certain conditions fine-grained graphite can also exhibit excellent fraction-specific DoG, when particle size reduction performed after full graphitization (following high-temperature treatment). In addition, post-graphitization fragmentation or exfoliation may preserve basal-plane stacking in graphite, compared to defect-generating mechanical milling (Suryanarayana, 2001; Hernandez et al., 2008; Inagaki & Kang, 2014).

3.3. Industrial implications

The experimental results confirm that the industrial-scale particle size fractionation acts as a structural sorting process, which preferentially concentrates defect-rich graphite in fine fractions rather than simply reducing particle dimensions. In addition, fine graphite fractions disproportionately influence surface-controlled phenomena such as solid-electrolyte interphase formation, enrichment of low-order graphite in fines may have a disproportionate impact on electrochemical performance (Xu, 2014). Therefore, size-resolved XRD analysis on graphite samples provides additional diagnostic insight for process optimization and troubleshooting.

Table 2. The concentration of the Graphite-1 & -2 in analyzed samples along with DoG value for each domain. Mass-weighted reconstructed bulk DoG values were calculated by weighting fraction-specific phase-weighted DoG values by the mass of each fraction recovered from a 3 g bulk split; XRD measurements were performed on ~1 g aliquots from each fraction to determine fraction-specific DoG values used in the reconstruction.

	Sample-01							
	Bulk Sample		**Particle Size class**					
			<75 µm		**75-150 µm**		**150-425 µm**	
	Graphite-I	Graphite-II	Graphite-I	Graphite-II	Graphite-I	Graphite-II	Graphite-I	Graphite-II
Diffraction weighted DoG*	**96.9**	**88.0**	**92.4**	**72.4**	**93.1**	**80.8**	**95.5**	**86.8**
Fraction-specific DoG	-		89.2		86.6		91.7	
Mass (g)	3.0		2.00		0.80		0.20	
Bulk phase-weighted DoG	93.1							
Mass-weighted reconstructed DoG	88.6							
ΔDoG	-4.5							
Relative Concentrations (Wt%)								
Graphite-I	25.0		25.0		14.5		23.6	
Graphite-II	18.9		4.8		16.5		18.7	
Int Amor**	56.1		70.3		69.0		57.7	

	Sample-02							
	Bulk Sample		**Particle Size class**					
			<75 µm		**75-150 µm**		**150-425 µm**	
	Graphite-I	Graphite-II	Graphite-I	Graphite-II	Graphite-I	Graphite-II	Graphite-I	Graphite-II
Diffraction weighted DoG*	95.2	86.8	95.5	88.4	96.4	86.2	97.2	86.4
Fraction-specific DoG	-		92.6		94.5		95.1	
Mass (g)	3.0		0.40		0.80		1.80	
Bulk phase-weighted DoG	90.1							
Mass-weighted reconstructed DoG	94.6							
ΔDoG	+4.5							
Relative Concentrations (Wt%)								
Graphite-I	33.1		50.9		68.4		34.4	
Graphite-II	52.1		34.6		15.7		8.3	
Int Amor**	14.8		14.5		15.9		57.3	

* Bulk DoG

**Amorphous content

4. Conclusions

In standard laboratory practice, clients most typically request bulk powder analysis for DoG determination, because it provides structurally meaningful diffraction-weighted averages and is economical, reproducible across independently prepared aliquots from the same batch, and suitable for quality control and comparative benchmarking. Graphite powders commonly exhibit size-dependent microstructural heterogeneity that reflects the coexistence of multiple stacking populations with different degrees of graphitization.

This study suggested a size-resolved XRD analysis as a complementary, value-added framework for diagnosing graphitization efficiency and processing-induced structural degradation. The validity of the proposed averaging framework is quantitatively demonstrated by mass-weighted reconstruction of bulk DoG values using particle-size–resolved data. The results confirm that reconstructed mass-weighted bulk DoG values are controlled by the mass distribution of structurally distinct graphite populations rather than fitting artefacts or preferred orientation effects. Mass-weighted reconstruction yield a representative bulk DoG value, allowing additional insight into how particle size distribution influences the overall graphitization in heterogeneous graphite powders.

Acknowledgements

This research was conducted within the context of AGAT geo-analytical laboratory providing routine XRD characterization services to clients across multiple sectors, including graphite exploration, processing, and production. The authors acknowledge the use of laboratory facilities and analytical instrumentation at AGAT Laboratories Ltd. This work was conducted as part of the authors' ongoing research and method development activities within the laboratory.

References

Biscoe, J., & Warren, B. E. (1942). An X-ray study of carbon black. J. Appl. Phys., 13, 364–371.

Chung, D. D. L. (2002). Review: graphite. J. Mater. Sci., 37, 1475–1489.

Bish, D.L., & Post, J.E. (1993). Quantitative Mineral Analysis Using the Rietveld Method. Reviews in Mineralogy, Vol. 20.

Dollase, W. A. (1986). Correction of intensities for preferred orientation. J. Appl. Cryst., 19, 267–272.

Franklin, R. E. (1951). Crystallite growth in graphitizing and non-graphitizing carbons. Proc. R. Soc. A, 209, 196–218.

Inagaki, M., & Kang, F. (2014). Materials Science and Engineering of Carbon. Butterworth-Heinemann.

Hernandez, Y., Nicolosi, V., Lotya, M., Blighe, F.M., Sun, Z., De, S., McGovern, I.T., Holland, B., Byrne, M., Gun'ko, Y.K., Boland, J.J., Niraj, P., Duesberg, G., Krishnamurthy, S., Goodhue, R., Hutchison, J., Scardaci, V., Ferrari, A.C., Coleman, J.N., 2008. High-yield production of graphene by liquid-phase exfoliation of graphite. Nature Nanotechnology 3, 563–568.

Klug, H. P., & Alexander, L. E. (1974). X-ray Diffraction Procedures: X-Ray Diffraction Procedures: For Polycrystalline and Amorphous Materials, 2nd Edition. Wiley. ISBN: 978-0-471-49369-3, P992.

Rietveld, H.M. (1969). A profile refinement method for nuclear and magnetic structures. Journal of Applied Crystallography, 2, 65–71.

Scarlett, N. V. Y., & Madsen, I. C. (2006). Quantification with overlapping diffraction peaks. Powder Diffraction, 21, 278–284.

Suryanarayana, C., 2001. Mechanical alloying and milling. Progress in Materials Science 46 (1–2), 1–184.

Young, R. A. (Ed.) (1993). The Rietveld Method. Oxford Univ. Press.

Xu, K. (2014). Electrolytes and interphases in Li-ion batteries. Chem. Rev., 114, 11503–11618. Warren, B. E. (1941). X-ray diffraction in random layer lattices. Phys. Rev., 59, 693–698.